# NIH RELAIS Document Delivery

NIH-10071777

NIH -- W1 NA81

PAMELA GEHRON ROBEY
CSDB/NIDR/NIH Bldng 30 Rm 228
30 CONVENT DRIVE MSC 4320
BETHESDA, MD 20892

ATTN:
PHONE: 301-496-4563
FAX: 301-402-0824
E-MAIL:

SUBMITTED: 2001-11-19 16:20:48
PRINTED: 2001-11-20 14:05:24
REQUEST NO.: NIH-10071777
SENT VIA: LOAN DOC
5052844

---

NIH Fiche to Paper Journal

---

| | |
|---|---|
| TITLE: | NATURE |
| PUBLISHER/PLACE: | Nature Publishing Group London : |
| VOLUME/ISSUE/PAGES: | 1994 Jun 23;369(6482):621-8 621-8 |
| DATE: | 1994 |
| AUTHOR OF ARTICLE: | Lambright DG; Noel JP; Hamm HE; Sigler PB; |
| TITLE OF ARTICLE: | Structural determinants for activation of the alph |
| ISSN: | 0028-0836 |
| OTHER NOS/LETTERS: | Library reports holding volume or year<br>0410462<br>8208289 |
| SOURCE: | PubMed |
| CALL NUMBER: | W1 NA81 |
| REQUESTER INFO: | AB424 |
| DELIVERY: | E-mail: probey@DIR.NIDCR.NIH.GOV |
| REPLY: | Mail: |

# Structural determinants for activation of the α-subunit of a heterotrimeric G protein

**David G. Lambright*, Joseph P. Noel*†, Heidi E. Hamm‡ & Paul B. Sigler*§**

* The Department of Molecular Biophysics and Biochemistry and the Howard Hughes Medical Institute, Yale University, 295 Congress Avenue, Boyer Center for Molecular Medicine, Room 154, New Haven, Connecticut 06510, USA
‡ Department of Physiology and Biophysics, University of Illinois at Chicago, Chicago, Illinois 60612, USA

**The 1.8 Å crystal structure of transducin α·GDP, when compared to that of the activated complex with GTP-γS, reveals the nature of the conformational changes that occur on activation of a heterotrimeric G-protein α-subunit. Structural changes initiated by direct contacts with the terminal phosphate of GTP propagate to regions that have been implicated in effector activation. The changes are distinct from those observed in other members of the GTPase superfamily.**

HETEROTRIMERIC guanine-nucleotide-binding proteins (G proteins; subunits $\alpha\beta\gamma$) function as molecular switches in a diverse set of signalling pathways by coupling seven-transmembrane-helix receptors (heptahelical receptors) to specific intracellular effectors. The transduction of signals depends on the ability of the $\alpha$-subunits to cycle between a resting (GDP-bound) conformation primed for interaction with agonist-stimulated receptors and an active (GTP-bound) conformation capable of activating or inhibiting a variety of downstream effectors including enzymes as well as ion channels[1,2]. In response to extracellular signals (such as hormones, neurotransmitters, opiates, odorants and light), heptahelical receptors catalyse the exchange of GTP for GDP, resulting in an active conformation with high affinity for specific downstream effectors and greatly reduced affinity for the $\beta\gamma$ subunits[3].

One of the best characterized heterotrimeric G-protein-coupled systems is the visual cascade of retinal rod outer segments[4–6]. Here, signal transduction begins with the absorption of a photon by the 11-*cis*-retinal chromophore of the photoreceptor rhodopsin (Rh). Rapid photoisomerization to all-*trans*-retinal triggers a series of structural changes that lead to the formation of the activated intermediate meta-rhodopsin II (Rh*). Rh* binds the heterotrimeric GDP-bound form of transducin ($G_{t\alpha\beta\gamma}$) and catalyses the exchange of GTP for GDP, resulting in the dissociation of $G_{t\alpha\beta\gamma}$ into $G_{t\alpha}$·GTP and $G_{t\beta\gamma}$. $G_{t\alpha}$·GTP, in turn, binds to and activates a potent cyclic GMP phosphodiesterase (PDE; subunits $\alpha\beta\gamma_2$) by displacing its inhibitory $\gamma$-subunits. The resulting decrease in second messenger cGMP concentration causes cation-specific cGMP-gated channels to close, leading to hyperpolarization of the rod outer segment membrane. As a result of an intrinsic GTPase activity, $G_{t\alpha}$ is inactivated by hydrolysis of GTP to GDP, returning the system to its resting state.

Heterotrimeric G proteins are members of a large superfamily of GTPases which mediate diverse processes such as cellular signalling, protein synthesis, vesicular trafficking and synaptic fusion[7]. Crystal structures of the GDP- and GTP-bound forms have been reported for two members of the GTPase superfamily, the monomeric G protein $p21^{ras}$ (Ras)[8–10] and the bacterial elongation factor EF-Tu[11,12,44]. In Ras, the conformational differences are restricted to the two regions of the protein that contact the $\gamma$-phosphate of GTP. In EF-Tu, by contrast, nucleotide exchange is accompanied by a large domain rearrangement.

To establish the nature of the conformational change induced by the exchange of GTP for GDP and the switch mechanism by which the presence or absence of the $\gamma$-phosphate defines the 'active' or 'inactive' state of a $G_\alpha$ subunit, it is necessary to compare the crystal structures of the GDP- and GTP-bound forms. We recently determined the structure of the active conformation of transducin-$\alpha$ complexed with a non-hydrolysable GTP analogue ($G_{t\alpha}$·GTP-γS)[13]. We now report the crystal structure of the inactive form, transducin-$\alpha$ complexed with GDP ($G_{t\alpha}$·GDP). The structures of both the active and inactive forms have been refined to a resolution of 1.8 Å, enabling us to describe in accurate detail the nature and mechanism of the conformational switch in a heterotrimeric G-protein $\alpha$-subunit and the functional implications for interaction with other components of the signalling cascade.

## Structure determination and refinement

A 325-amino-acid proteolytic fragment (lacking the first 25 amino acids) of bovine retinal rod outer segment $G_{t\alpha}$, complexed with either GDP or GTP-γS and suitable for crystallization, was prepared by limit digestion with a lysine-specific protease, endoproteinase lysC[14]. To prevent additional cleavage during limit digestion, $G_{t\alpha}$·GDP was reversibly activated with aluminium fluoride[15] which was subsequently removed by ultrafiltration. Crystals of $G_{t\alpha}$·GDP in the orthorhombic space group *I*222 were grown at 4 °C from sodium 2-(*N*-morpholino)ethanesulphonate(MES)-buffered solutions (pH 6.0) containing 10% polyethylene glycol-8000 (PEG 8000), 10% glycerol, and 0.2 M, $MgCl_2$. Monoclinic crystals of $G_{t\alpha}$·GTP-γS (space group $P2_1$; 3 complexes per asymmetric unit) were grown as described[13].

The crystal structure of $G_{t\alpha}$·GDP was solved at 4 Å by molecular replacement using the $G_{t\alpha}$·GTP-γS structure refined at 2.2 Å resolution[13] as a search model (Table 1). Both structures have been independently refined with simulated annealing against data which are >90% complete from 8.0 to 1.8 Å resolution (Table 1). The present model for $G_{t\alpha}$·GDP includes 314 residues from 27–340, a GDP molecule, a $Mg^{2+}$ ion, 339 water molecules and has a final *R*-value of 21.1% for all data (18.7% for data >2σ) and a free *R*-value of 23.6% (21.1% for data >2σ) for a randomly selected subset (10%) of the data omitted before the start of refinement. An example of the $2F_o-F_c$ electron density map is shown in Fig. 2*c*. Intensities for $G_{t\alpha}$·GTP-γS were collected and the refinement extended from the 2.2 Å resolution limit reported previously to the present resolution of 1.8 Å (Table 1). The current model for $G_{t\alpha}$·GTP-γS, which covers all three complexes in the asymmetric unit, includes 952 residues (26–342 for protomers a and b; 26–343 for protomer c), three

§ To whom correspondence should be addressed.
† Present address: Structural Biology Laboratory, The Salk Institute for Biological Studies, PO Box 85800 San Diego, California 92186–5800, USA.

GTP-$\gamma$S molecules, three $Mg^{2+}$ ions, 1,226 water molecules and has a final $R$-value of 22.9% for all data (21.1% for data $>2\sigma$), and a free $R$-value of 27.6% (25.8 for data $>2\sigma$). Both structures have excellent stereochemistry and $\phi$–$\psi$ angles within 10° of allowed regions of the Ramachandran plot. Procedural details of the structure solution and refinement are given in the legend of Table 1.

## Overall structure and nucleotide binding

The fold of $G_{t\alpha}$, whether complexed with GDP or GTP-$\gamma$S, consists of two domains (Fig. 1), a GTPase domain common to members of the GTPase superfamily and an $\alpha$-helical domain unique to the highly homologous family of heterotrimeric G-proteins[13]. The GTPase domain consists of five helices ($\alpha$1–$\alpha$5) surrounding a six-stranded $\beta$-sheet ($\beta$1–$\beta$6) with five strands running parallel and one ($\beta$2) running antiparallel to the others. In contrast to Ras and EF-Tu, the second of the five helices in $G_{t\alpha}$ ($\alpha$2) is a $3_{10}$ helix rather than an $\alpha$-helix. The helical domain has an entirely $\alpha$-helical secondary structure with one long central helix ($\alpha$A) surrounded by five shorter helices ($\alpha$B–$\alpha$F) and is linked to the GTPase domain by two extended strands, linker 1 (54–58) and linker 2 (173–179). Between these two domains lies a deep cleft within which the nucleotide is tightly bound.

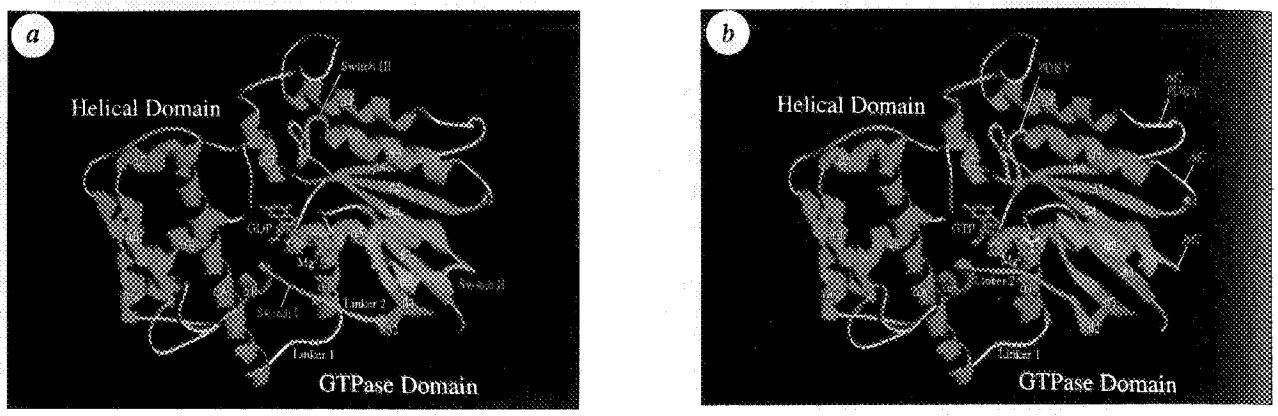


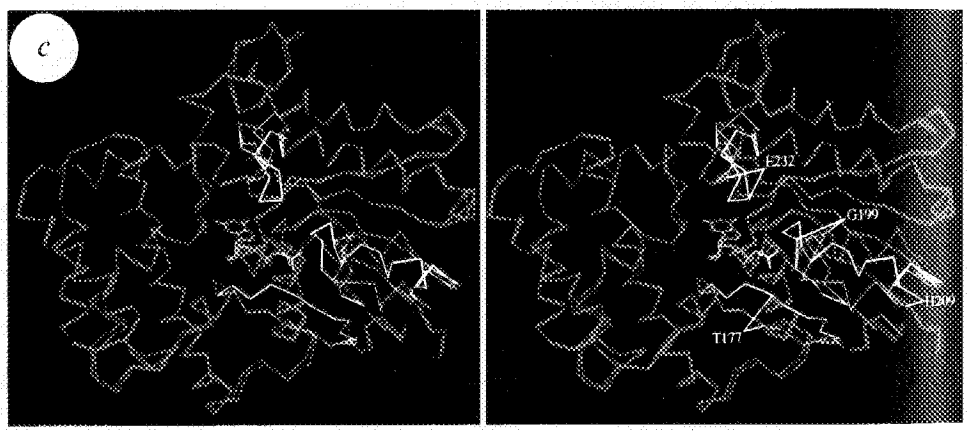


FIG. 1 Structural differences between the inactive and active forms of $G_{t\alpha}$. *a*, Ribbon drawing of $G_{t\alpha}$·GDP (inactive conformation) with the three switch regions (I, II and III) highlighted in blue and the GDP in purple. *b*, Ribbon drawing of $G_{t\alpha}$·GTP-$\gamma$S (active conformation) with the switch regions highlighted in blue, GTP-$\gamma$S in purple, and the $\gamma$-phosphate in yellow. The two loop regions that have been implicated in the interaction $G_{t\alpha}$ with PDE$\gamma$ (see text) are indicated with yellow labels. Also shown (purple labels) are the corresponding locations in $G_{t\alpha}$ of the three loop regions that have been implicated in the interaction of $G_{s\alpha}$ with adenylyl cyclase (AC). *c*, Stereo view showing the C$\alpha$ traces of the GDP- and GTP-$\gamma$S-bound forms of $G_{t\alpha}$ superimposed by least-squares and oriented as in *a*. Both molecules are shown in green except for the switch regions which are highlighted in cyan for the GDP-bound form and yellow for the GTP-$\gamma$S-bound form. The labels indicate the respective locations of selected $\alpha$ carbons in the two conformations. *d*, Stereo view of the $G_{t\alpha}$·GDP and $G_{t\alpha}$·GTP-$\gamma$S C$\alpha$ traces rotated about a vertical axis by ~90° relative to the view in *c*. The $\alpha$ carbons of R204, K205 and K206 are indicated by white, red and green circles, respectively. Note the ~90° rotation of these residues on going from the inactive (cyan) to the active (yellow) conformation. *e*, Primary sequence alignment. Residues in the three switch regions are highlighted in light blue. Residues involved in conserved contacts to the $\gamma$-phosphate and switch II region are indicated by blue and red boxes, respectively. The corresponding secondary structure for the $G_{t\alpha}$·GDP is shown below the aligned sequences. Sources of sequence information: bovine $G_{t\alpha}$[32], bovine $G_{s\alpha}$[33], bovine $G_{i\alpha}$[34], bovine $G_{o\alpha}$[35], mouse $G_{q\alpha}$[36], human $G_{z\alpha}$[37], yeast $G_{\alpha 1}$[38], p21 Ras[39] and EF-Tu[40].

Noel *et al.*[13] suggested that the presence of the helical domain is the barrier that accounts for the slow rate of intrinsic nucleotide exchange ($\sim 10^{-3}$ min$^{-1}$ at 30 °C for $G_{t\alpha}$ (ref. 41)), allowing it to be controlled by the catalytic action of an activated receptor. In heterotrimeric G proteins, GDP release is independent of $Mg^{2+}$ concentration[42], whereas in Ras which lacks the helical domain, GDP release is highly dependent on $Mg^{2+}$ concentration[43] (500-fold faster in nM than in mM $Mg^{2+}$).

In addition to the bound nucleotide, both structures show clear density for a $Mg^{2+}$ ion with six ligands coordinated in octahedral geometry. In the $G_{t\alpha} \cdot$ GTP-$\gamma$S structure, the nucleotide is essentially occluded from the bulk solvent and the $Mg^{2+}$ ion coordinates oxygens from the $\beta$- and $\gamma$-phosphates, the side chains of Ser 43 and Thr 177, and two water molecules[13]. In the $G_{t\alpha} \cdot$ GDP structure, however, two of the ligands, the $\gamma$-phosphate oxygen and the side-chain oxygen of Thr 177, are replaced by water molecules. In addition, both linker 2 and the $\beta 3$–$\alpha 2$ loop are displaced from their respective locations in the $G_{t\alpha} \cdot$ GTP-$\gamma$S structure, resulting in greater solvent exposure in the vicinity of the $\beta$-phosphate and $Mg^{2+}$ ion. The other

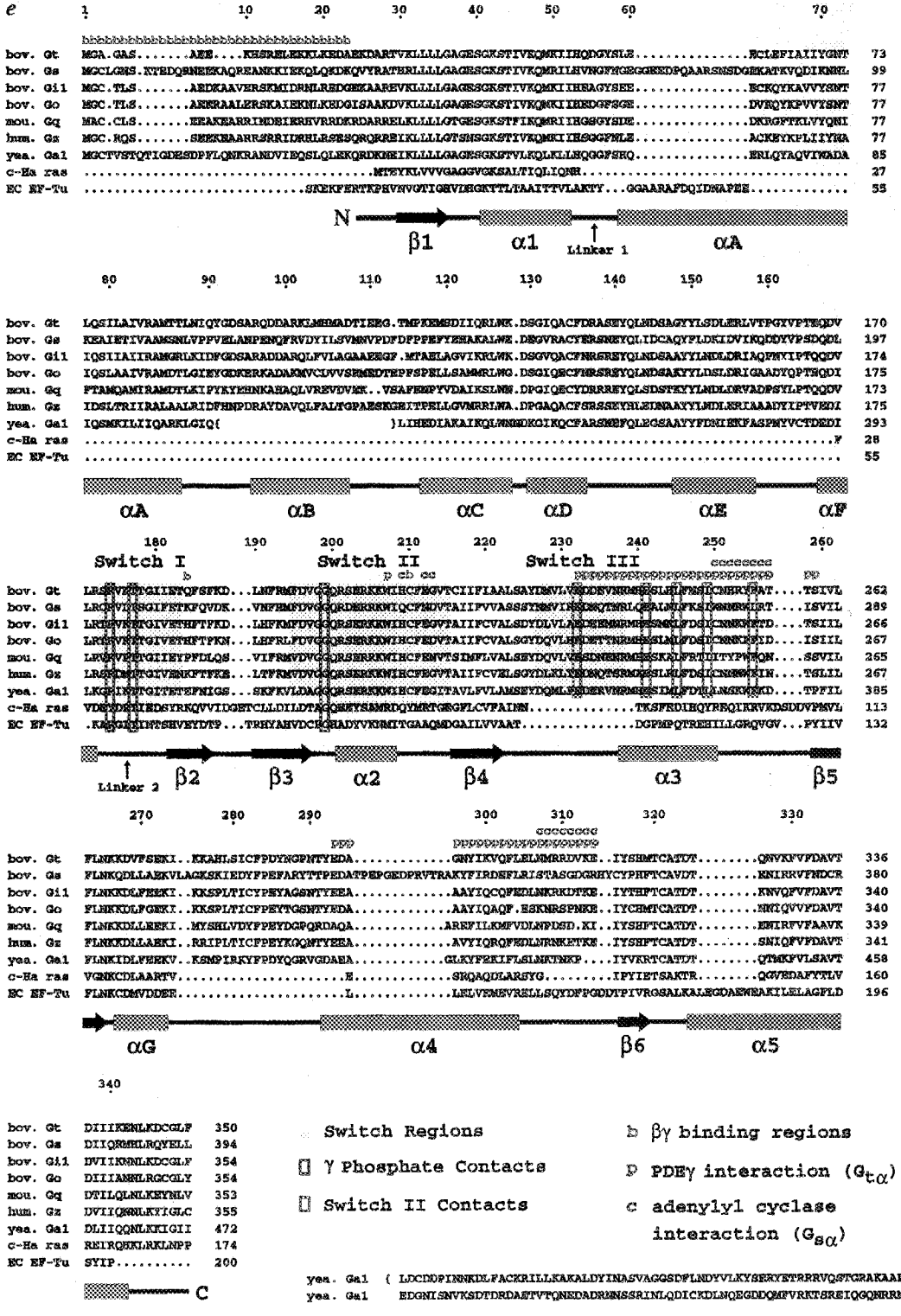

TABLE 1 Structure determination and refinement

| Search structure | Rotation search: Euler angles $\Theta_1$ | $\Theta_2$ | $\Theta_3$ | Refined PC(Ω): Highest peak | Highest False Peak |
|---|---|---|---|---|---|
| GTPase domain | 60.9 | 65.2 | 42.1 | 6.4σ | 3.8σ |
| Helical domain | 59.4 | 62.9 | 47.8 | 6.9σ | 5.1σ |
| Both domains | 60.0 | 65.8 | 43.2 | 6.8σ | 2.3σ |

| Space group | Translation search: Fractional Coordinates $x$ | $y$ | $z$ | Refined PC(Ω): Highest peak | Highest false peak |
|---|---|---|---|---|---|
| I222 | 0.43 | 0.40 | 0.34 | 23σ | 15σ |
| $I2_12_12_1$ | 0.43 | 0.14 | 0.37 | 16σ | 16σ |

| $G_{t\alpha}$·GDP refinement | | | | | | | | |
|---|---|---|---|---|---|---|---|---|
| Resolution limit (Å) | 3.51 | 2.83 | 2.48 | 2.26 | 2.10 | 1.98 | 1.88 | 1.80 | Total |
| Number of reflections | 5,382 | 5,285 | 5,208 | 5,216 | 5,164 | 5,123 | 5,124 | 4,569 | 41,071 |
| % Complete | 100 | 100 | 100 | 99.9 | 99.7 | 99.1 | 98.8 | 88.9 | 98.3 |
| $\langle I/\sigma \rangle$ | 31.4 | 26.6 | 19.7 | 14.7 | 10.7 | 7.60 | 4.85 | 3.42 | 19.0 |
| $R_{sym}$ | 0.086 | 0.102 | 0.125 | 0.163 | 0.201 | 0.272 | 0.403 | 0.542 | 0.124 |
| *R*-factor (all data) | 0.198 | 0.178 | 0.198 | 0.207 | 0.217 | 0.234 | 0.283 | 0.331 | 0.211 |
| *R*-factor (date>2.0σ) | 0.194 | 0.169 | 0.184 | 0.185 | 0.188 | 0.192 | 0.204 | 0.218 | 0.187 |
| Free *R*-factor (all data) | 0.231 | 0.203 | 0.219 | 0.222 | 0.236 | 0.267 | 0.320 | 0.350 | 0.236 |
| Free *R*-factor (data>2.0σ) | 0.226 | 0.195 | 0.199 | 0.207 | 0.209 | 0.214 | 0.229 | 0.226 | 0.211 |
| r.m.s. deviations | Bond lengths 0.010 | | Bond angles 1.46 | | | | | | |

| $G_{t\alpha}$·GTP-γS refinement | | | | | | | | |
|---|---|---|---|---|---|---|---|---|
| Resolution limit (Å) | 3.51 | 2.83 | 2.48 | 2.26 | 2.10 | 1.98 | 1.88 | 1.80 | Total |
| Number of reflections | 13,384 | 13,193 | 12,874 | 12,407 | 12,093 | 11,768 | 11,506 | 11,367 | 98,592 |
| % Complete | 98.9 | 98.3 | 96.2 | 92.7 | 90.5 | 88.1 | 86.2 | 85.1 | 92.0 |
| $\langle I/\sigma \rangle$ | 27.2 | 25.6 | 18.9 | 14.1 | 10.9 | 7.97 | 5.24 | 3.38 | 20.4 |
| $R_{sym}$ | 0.064 | 0.067 | 0.082 | 0.104 | 0.132 | 0.172 | 0.243 | 0.337 | 0.077 |
| *R*-factor (all data) | 0.175 | 0.189 | 0.226 | 0.253 | 0.273 | 0.315 | 0.382 | 0.469 | 0.229 |
| *R*-factor (date>2.0σ) | 0.175 | 0.187 | 0.218 | 0.239 | 0.25 | 0.271 | 0.290 | 0.301 | 0.211 |
| Free *R*-factor (all data) | 0.239 | 0.243 | 0.273 | 0.290 | 0.295 | 0.329 | 0.402 | 0.518 | 0.276 |
| Free *R*-factor (data>2.0σ) | 0.239 | 0.241 | 0.266 | 0.276 | 0.278 | 0.289 | 0.299 | 0.319 | 0.258 |
| r.m.s. deviations | Bond lengths 0.008 Å | | Bond angles 1.31° | | | | | | |

$G_{t\alpha\beta\gamma}$ was isolated from photolysed bovine retinal rod outer segments (ROS) by selective extraction with GTP as described[27]. $G_{t\alpha}$·GDP was separated from $G_{t\beta\gamma}$ by chromatography on a cibacron blue column (HiTrap Blue, Pharmacia; 10 mM Tris, pH 7.5, 6 mM $Mg_2SO_4$, 1 mM EDTA, 10% glycerol, 0.1% β-mercaptoethanol, step to 0.15 M NaCl for 23 column volumes to elute $G_{t\beta\gamma}$, and 0.15–1 M NaCl gradient over 10 column volumes to elute $G_{t\alpha}$·GDP). A 325 amino-acid fragment (residues 26–350) of $G_{t\alpha}$·GDP was prepared by endoproteinase LysC (Boehringer Mannheim) digestion of the full-length protein, reversibly activated with aluminium flouride (50 μM $AlCl_3$ and 15 mM NaF), for 12 h at 4 °C in 10 mM Tris, pH 7.5, 0.5 mM $MgCl_2$, 10% glycerol, and 0.1% β-mercaptoethanol. The proteolytic fragment was then purified on Mono-Q (10 mM Tris, pH 7.5, 0.5 mM $MgCl_2$, 50 μM $AlCl_3$, 15 mM NaF, 10% glycerol, 0.1% β-mercaptoethanol, and 0.1–0.2 M NaCl gradient over 30 column volumes) in the presence of aluminium fluoride which was subsequently removed by ultrafiltration. Diffraction quality crystals of $G_{t\alpha}$·GDP in the orthorhombic space group I222 were grown at 4 °C in microseeded hanging drops containing 13.3 mg $ml^{-1}$ protein, 6% PEG-8000, 6.67% glycerol, 33.3 mM MES, pH 6.0, 133 mM $MgCl_2$, and 0.1% β-mercaptoethanol equilibrated against a reservoir of 9% PEG-8000, 10% glycerol, 50 mM MES, pH 7.5, 200 mM $MgCl_2$, and 0.1% β-mercaptoethanol. Crystals appeared within 2 days and grew to maximum dimensions of 0.05 × 0.2 × 0.5 mm in 1–2 weeks. The unit cell dimensions are $a = 71.9$, $b = 87.8$, $c = 143.1$ Å. Crystals were stabilized in a cryosolution consisting of 20% PEG-8000, 30% glycerol, 200 mM $MgCl_2$, and 0.1%β-mercaptoethanol and flash frozen in liquid nitrogen-cooled liquid propane. Diffraction data to 1.8 Å for $G_{t\alpha}$·GDP and $G_{t\alpha}$·GTP-γS were collected at the X-25 beamline of the National Synchrotron Light Source at Brookhaven National Laboratory, processed with DENZO (Z. Otwinowski), and scaled with SCALEPACK (Z. Otwinowski). Rotation searches with the GTPase and helical domains either separately or together gave similar solutions after Patterson correlation refinement[28], indicating that the two domains have the same relative orientation in both structures. A translation search using both domains yielded a clear solution in the space group I222 (but not $I2_12_12_1$) with an *R*-value of 45% after rigid body refinement. Inspection of the difference electron density maps ($2F_o$–$F_c$ and $F_o$–$F_c$) at this stage indicated several regions with poor density for main-chain atoms. These regions were removed from the initial model which was then refined in stages of increasing resolution (from 2.8 to 1.8 in steps of 0.2 Å) using a simulated annealing protocol with an initial temperature of 4,000 K. All computations for molecular replacement and subsequent refinement were done with X-PLOR 3.1[29]. Interactive model building was done with the programs O[30] or Frodo[31].

$$PC(\Omega) = \frac{\langle |E_{obs}|^2 |E_m(\Omega)|^2 \cdots \langle |E_{obs}|^2 | \rangle \langle |E_m(\Omega)|^2 \rangle \rangle}{[\langle |E_{obs}|^4 - \langle |E_{obs}|^2 \rangle^2 \rangle \langle |E_m(\Omega)|^4 - \langle |E_m(\Omega)|^2 \rangle^2 \rangle]^{1/2}}$$

where $E_{obs}$ denotes the normalized observed structure factors and $E_m$ denotes the normalized structure factors for the search model placed in a triclinic unit cell with geometry identical to that of the crystal[28].

$R_{sym} = \sum_{h'} \langle |I_h - I_{h'}| \rangle / \sum_{h'} I_{h'}$ where $\langle |I_h - I_{h'}| \rangle$ is the average of the absolute deviation of a reflection $I_{h'}$ from the average $I_h$ of its symmetry and Friedel equivalents.

hydrogen-bonding and van der Waals contacts to the base, ribose, and α- as well as β-phosphates are nearly identical in both structures.

## Activation of an α-subunit

As shown in Fig. 1, the structures of $G_{t\alpha}$·GDP and $G_{t\alpha}$·GTP-γS are quite similar. In fact, if the switch regions described below are excluded, the r.m.s. deviation after superposition of the remaining 281 Cα atoms is only 0.8 Å. Thus, to a good approximation, the structural differences induced by nucleotide exchange are localized to three adjacent regions on one face of the protein (Fig. 1). Subsequently, we will refer to these regions as switch I, II and III. Switch I (Ser 173–Thr 183) encompasses linker 2 and extends partially into the β2 strand. Switch II (Phe 195–Thr 215) begins near the C terminus of β3, extends through α2, and includes the α2–β4 loop. Switch III (Asp 227–Arg 238) spans the β4–α3 loop and occurs within a sequence segment (I2) that is the second of four sequence inserts (I1–I4) with respect to the Ras sequence. The switch I and II regions have counterparts in Ras[8–10] and EF-Tu[11,12,44] by virtue of similar contacts between the γ-phosphate of GTP and two highly conserved residues, Thr 177 in switch I and Gly 199 in switch II. Switch III, by contrast, is unique to heterotrimeric G proteins and the conformational changes in this region (described below) appear to occur as a secondary response propagated from switch II through a network of interactions, primarily ionic, that are conserved in heterotrimeric G proteins. With the exception of a short stretch of residues (Gln 143–Asn 145) which in $G_{t\alpha}$·GTP-

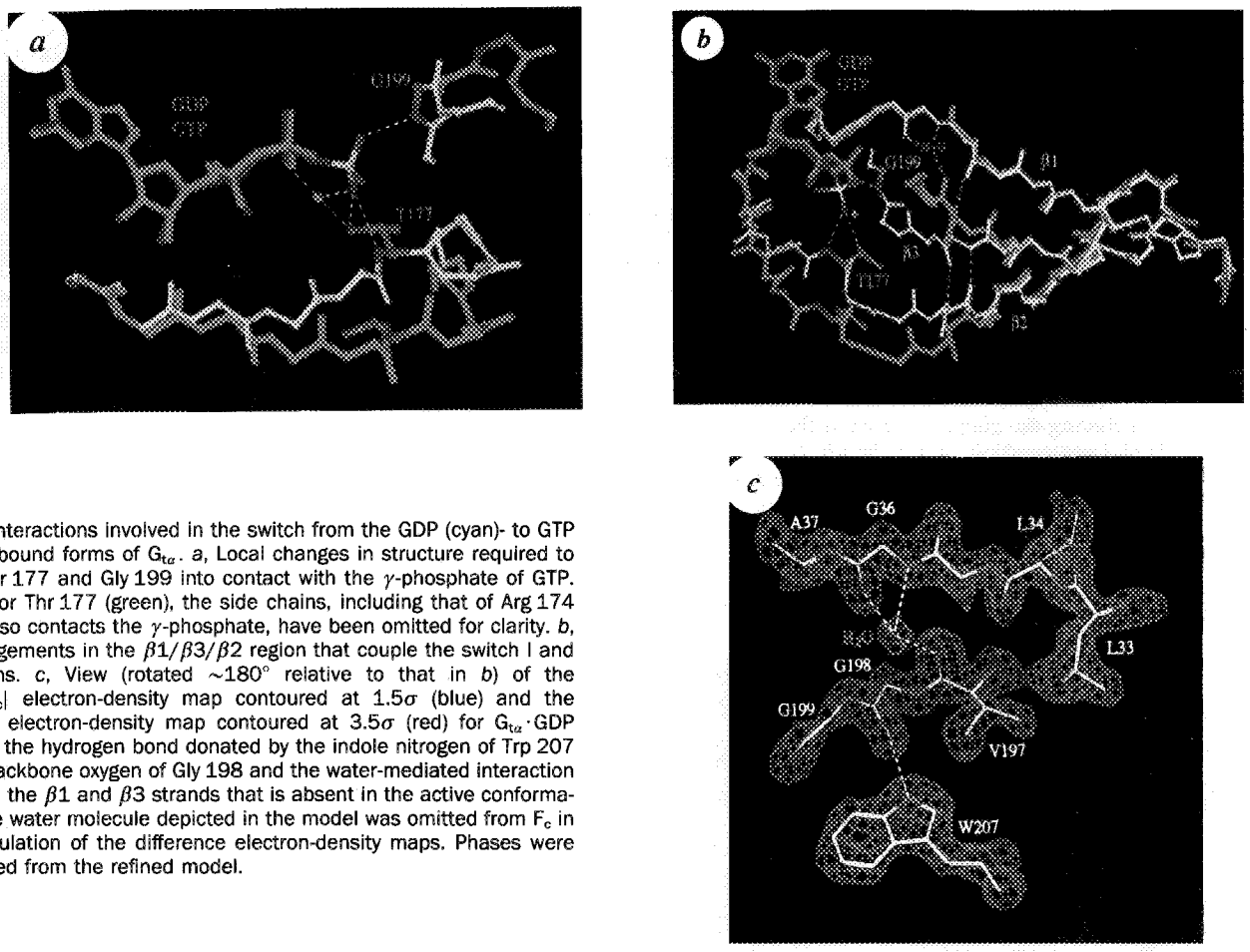


FIG. 2 Interactions involved in the switch from the GDP (cyan)- to GTP (yellow)-bound forms of $G_{t\alpha}$. *a*, Local changes in structure required to bring Thr 177 and Gly 199 into contact with the $\gamma$-phosphate of GTP. Except for Thr 177 (green), the side chains, including that of Arg 174 which also contacts the $\gamma$-phosphate, have been omitted for clarity. *b*, Rearrangements in the $\beta1/\beta3/\beta2$ region that couple the switch I and II regions. *c*, View (rotated ~180° relative to that in *b*) of the $2|F_o|-|F_c|$ electron-density map contoured at $1.5\sigma$ (blue) and the $|F_o|-|F_c|$ electron-density map contoured at $3.5\sigma$ (red) for $G_{t\alpha}\cdot$GDP showing the hydrogen bond donated by the indole nitrogen of Trp 207 to the backbone oxygen of Gly 198 and the water-mediated interaction between the $\beta1$ and $\beta3$ strands that is absent in the active conformation. The water molecule depicted in the model was omitted from $F_c$ in the calculation of the difference electron-density maps. Phases were calculated from the refined model.

$\gamma$S lie in contact with the switch III region, both the conformation of the helical domain and its orientation with respect to the GTPase domain are essentially unaffected by nucleotide exchange. Likewise, the I3 and I4 regions are also unchanged.

Structural changes in the switch I region are induced by hydrogen bonds between the $\gamma$-phosphate of GTP and Thr 177 (Fig. 2*a*) and to a lesser degree the cholera toxin-sensitive residue Arg 174. Specifically, the O3 oxygen of the $\gamma$-phosphate accepts hydrogen bonds from both the main-chain N and side-chain OH of Thr 177, the oxygen of which is also coordinated to the $Mg^{2+}$ ion, whereas the $\gamma$-S interacts with the guanidylyl group of Arg 174. The structural changes occurring in the switch I region are conceptually simple. After nucleotide exchange, linker 2 is drawn essentially as a whole towards the $\gamma$-phosphate, bringing the side chain oxygen of Thr 177 into the coordination sphere of the $Mg^{2+}$ ion where it replaces one of the water ligands observed in the structure of the GDP form. The average main chain *B*-factor for residues in the switch I region is a factor of 2 lower in the $G_{t\alpha}\cdot$GTP-$\gamma$S structure, suggesting the importance of the stabilizing contacts with the $\gamma$-phosphate and $Mg^{2+}$ ion to the active conformation.

Changes in the switch II region are initiated by a hydrogen bond between the peptide NH of Gly 199 and the $\gamma$-phosphate of GTP (Fig. 2*a*). Gly 199 is located in a short loop preceding $\alpha2$ which in $G_{t\alpha}\cdot$GDP forms a severely distorted 3–10 helix that terminates in a type I reverse turn stabilized by a salt bridge between His 209 and Glu 212. Movements in this loop are coupled to structural changes in $\alpha2$ through a hydrogen bond from the indole NH of Trp 207 to the backbone carbonyl of Gly 198 (Fig. 2*c*). To bring Gly 199 into contact with the $\gamma$-phosphate of GTP, the switch II region is both stretched and rotated (roughly a quarter turn anticlockwise when viewed from the phosphate) relative to its conformation in $G_{t\alpha}\cdot$GDP. The net effects are to: (1) straighten $\alpha2$ into a more ideal 3-10 helix (Fig. 1*c*, *d*); (2) disrupt the reverse turn at the end of $\alpha2$ and the associated interaction between His 209 and Glu 212 (Fig. 3*c*, *d*); (3) bring the exposed side chains of the conserved residues Arg 201, Arg 204 and Trp 207 into contact with conserved residues in $\alpha3$ that are unique to heterotrimeric G proteins (Fig. 3*a*, *b*). In $G_{t\alpha}\cdot$GTP-$\gamma$S, the guanadinium groups of Arg 201 and Arg 204 ion pair with the carboxylate group of Glu 241, whereas Trp 207 is buried between the side chains of Leu 245 and Ile 249. A further consequence of the conformational twist in the switch II region is that the end of $\beta3$ (from Phe 195 to Gly 199) pulls away from $\beta1$, disrupting one direct and one water-mediated hydrogen bond (Fig. 2*b*). These disrupted interactions are replaced by two new hydrogen bonds between $\beta3$ (the strand preceding Gly 199 in switch II) and $\beta2$ (the strand following linker 2 in switch I). The new hydrogen bonds couple the structural changes in the switch I and II regions, thereby lending cooperativity to the switch mechanism. Contrary to our initial expectations[13], the structural changes in the switch II region do not propagate to $\alpha3$. Instead, it appears that $\alpha3$ serves as a rigid scaffold for residues involved in stabilizing the active conformation of the switch II region.

The changes in the switch II region explain a variety of observations regarding the conformation of this region in solution. For example, proteolysis studies show that $G_{t\alpha}\cdot$GDP is sensitive to cleavage by trypsin[16] at Arg 204 and chymotrypsin[17] at Trp 207, whereas both sites are protected against proteolysis in the GTP conformation. Likewise, the amplitude of tryptophan fluorescence for $G_{t\alpha}\cdot$GTP-$\gamma$S is enhanced relative to that for $G_{t\alpha}\cdot$GDP consistent with one of transducin-$\alpha$'s two tryptophans having a more polar environment in the GDP conformation[18]. Mutation of Trp 207 to Phe eliminates the fluorescence change associated with activation[19]. Both results would be expected

from the switch II structural changes which rotate the Arg 204 and Trp 207 side chains from solvent-exposed conformations into ordered interactions with residues from $\alpha$3 and switch III.

Switch III responds to switch II by forming an elaborate interdependent network of polar interactions (Fig. 3*c*, *d*) with functional groups that have been positioned and firmly buttressed by the GTP-induced rearrangements in the switch II region. The carboxylate group of the conserved Glu 232 in switch III plays a crucial role by forming a direct interaction with the backbone amide of Arg 201 as well as water-mediated interactions with the guanidino NH of Arg 204 and the carbonyl oxygen of Gly 199 (Fig. 3*d*).

All of the critical residues for the conformational switch in $G_{t\alpha}$ are also present in the other heterotrimeric G-protein $\alpha$-subunits. Consequently, we anticipate that the same basic switch mechanism, including the coupling between the switch I and II regions and the propagation of the switch II changes to the switch III region, will hold for all members of the heterotrimeric G-protein family.

## Implications for 'release' of activated $G_\alpha$

A characteristic consequence of nucleotide exchange in heterotrimeric G proteins is reduced affinity of activated $G_\alpha$ for $G_{\beta\gamma}$. Extensive studies of the Gly 226 to Ala mutation in $G_{s\alpha}$ (Gly 199 in $G_{t\alpha}$), first identified as the H21A clone in S49 cells[20] and later introduced as a site-specific mutation[21], demonstrate that release of $G_{\beta\gamma}$ is a necessary event accompanying $G_\alpha$ activation and that the conformational changes in switch II are important for regulating affinity for $G_{\beta\gamma}$. In neither conformation does Gly 199 violate the $\phi\psi$ angles permitted by residues with c$\beta$ substituents. However, a c$\beta$ substituent cannot be tolerated at this position because it would result in an unfavourable steric interaction with the carbonyl oxygen of Gly 36 in the GTP but not in the GDP conformation. Figure 4 shows that the GDP-bound form has a cavity, formed by switch II, $\alpha$3 and switch III residues, that closes in response to the GTP-induced changes described above. The polar and non-polar residues in $\alpha$2 protrude as an open flap in the GDP-bound form and present a potential binding site for $G_{\beta\gamma}$ that would be lost on nucleotide exchange. One region of $G_\alpha$ important for binding to $G_{\beta\gamma}$ is the N terminus (see ref. 3) which is missing in our proteolysed form of $G_{t\alpha}$. A region adjacent to $\alpha$2 has been implicated in $G_{\beta\gamma}$ binding by a second site revertant at position 307 in the yeast mating factor $G_\alpha$ (corresponding to Gln 184 in $G_{t\alpha}$) which restores affinity for $G_{\beta\gamma}$ mutants that otherwise fail to interact properly with $G_\alpha$[22,23]. Moreover, a cysteine in the switch II

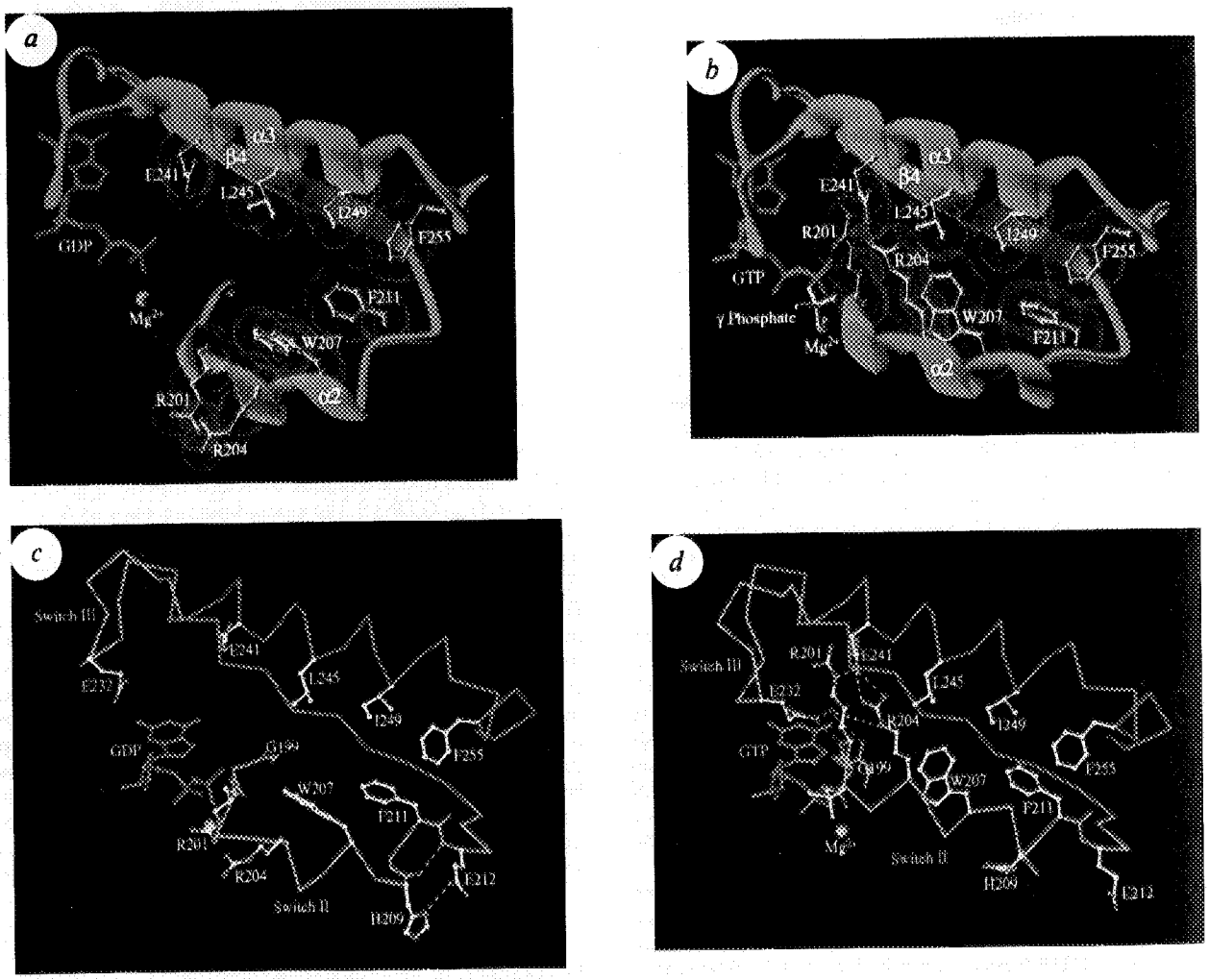


FIG. 3 Conformational changes in the switch II and III regions showing how the side chains of residues in $\alpha$2 rotate from solvent-exposed orientations in the inactive (GDP-bound) conformation to form an extensive interface with residues from the $\beta$4–$\alpha$3 loop and $\alpha$3 in the active (GTP-$\gamma$S-bound) conformation. *a*, Ribbon drawing of the $\alpha$2–$\alpha$3 region in $G_{t\alpha}$·GDP depicting the solvent-exposed side chains of the highly conserved residues Arg 201, Arg 204, Trp 207 and Phe 211 in $\alpha$2 and Glu 241, Leu 245, Ile 249 and Phe 255 in $\alpha$3. The GDP is coloured purple and the $Mg^{2+}$ ion appears as an orange sphere. *b*, Ribbon drawing of the a2–$\alpha$3 region in $G_{t\alpha}$·GTP-$\gamma$S showing the extensive interface formed between the side chains of residues in $\alpha$2 and $\alpha$3. *c*, Skeletal model of the $\alpha$2–$\alpha$3 region showing $\alpha$ carbons and selected side chains in $G_{t\alpha}$·GDP. *d*, Same view as c showing the interactions between the Glu 232 carboxylate and the backbone NH of Arg 201 (direct hydrogen bond) and the carbonyl of Gly 199 (water mediated) that couple switch III to switch II.

region of $G_{o\alpha}$ (Cys 210 in $G_{t\alpha}$) can be chemically crosslinked to bound $G_{o\beta\gamma}$[24]. In the context of the structural changes, these studies suggest that the switch II and perhaps the switch I region may play a role in modulating affinity for the $\beta\gamma$ subunits. The concomitant decrease in affinity for receptor could result from either a direct interaction of the receptor with one of the switch regions of $G_\alpha$ or, alternatively, as a consequence of the decreased affinity for $G_{\beta\gamma}$.

## Implications for effector activation

At least one of the regions involved in effector interaction must undergo conformational changes on nucleotide exchange. For two well characterized $G_\alpha$–effector interactions, $G_{t\alpha}\cdot$GTP activation of cGMP phosphodiesterase (cGMP PDE) and $G_{s\alpha}\cdot$GTP activation of adenylyl cyclase, effector activation regions have been inferred from biochemical[25] and mutational data[19,26]. Together these studies define a contiguous surface consisting of residues from $\alpha2$, $\alpha3$, the latter part of $\alpha4$, and the four loops $\alpha2$–$\beta4$, $\alpha3$–$\beta5$, $\alpha4$–$\beta6$, and $\beta4$–$\alpha3$ (see Fig. 4 of ref. 13). Of these, two occur within switch regions; the $\alpha2$–$\beta4$ loop lies at the end of switch II and the $\beta4$–$\alpha3$ loop corresponds to the switch III region.

$G_{t\alpha}\cdot$GTP activates cGMP PDE by binding to and displacing its inhibitory $\gamma$-subunits[4]. Studies with synthetic peptides have implicated two segments of $G_{t\alpha}$ in binding to PDE$\gamma$. A peptide, encompassing $\alpha4$ and the $\alpha4$–$\beta6$ loop, binds PDE$\gamma$ (dissociation constant, $K_d \sim 2\ \mu M$) and activates PDE[25]. However, we do not observe significant conformational changes in the $\alpha4$–$\beta6$ activating region (293–314). In fact, the $\alpha4$–$\beta6$ loop appears to be quite flexible in both nucleotide-bound forms of $G_{t\alpha}$, as shown by equally large main chain B-factors ($\langle B\rangle \sim 50$). A second peptide, beginning in the switch III region and extending through $\alpha3$, binds PDE$\gamma$ but does not activate PDE (J. Mills, manuscript in preparation). Switch III contains a cluster of acidic residues Glu 232-Asp-Asp-Glu 235 that could potentially interact with the highly basic central segment of PDE$\gamma$. Mutational studies have also implicated a switch II residue, Trp 207, in the interaction with PDE$\gamma$[19].

*In vivo* studies with $G_{i\alpha}$–$G_{s\alpha}$ chimaeras have implicated three loops, $\alpha2$–$\beta4$, $\alpha3$–$\beta5$, and $\alpha4$–$\beta6$, in $G_{s\alpha}$ activation of adenylyl cyclase[26]. Of these only the $\alpha2$–$\beta4$ loop exhibits a clearly identifiable structural change on nucleotide exchange. Indeed the sequence segment of $G_{i\alpha}$ that was inserted in the $\alpha2$–$\beta4$ loop is identical to that of $G_{t\alpha}$ and maps directly onto the reverse turn at the end of $\alpha2$ (see Fig. 1*e*), suggesting a plausible mechanism for $G_{s\alpha}$ activation of adenylyl cyclase in which disruption of this reverse turn on nucleotide exchange releases residues that, with the other effector interaction regions of $G_{s\alpha}$, cooperatively enhance affinity for adenylyl cyclase.

## Comparison with p21 Ras and EF-Tu

The switch I and II regions of $G_{t\alpha}$ are analogous to switch regions in Ras[8–10] and EF-Tu[11,12,44] whereas switch III is unique to the heterotrimeric family of G proteins. Aside from the conserved threonine and glycine residues, the switch I and II regions exhibit little if any sequence similarity to the corresponding switch regions of Ras or EF-Tu and, despite highly conserved contacts with the $\gamma$-phosphate of GTP, both the nature and extent of the resulting structural changes are quite distinct. In $G_{t\alpha}$, the changes in the switch I region begin at Ser 173, extend through linker 2, and include a portion of $\beta3$. Nucleotide exchange is accompanied by movement of the whole of this region. In Ras, by contrast, the key element of the switch I conformational rearrangement is a 180° flip of the peptide backbone bringing Thr 35 (corresponding to Thr 177 in $G_{t\alpha}$) from a solvent-exposed orientation in the GDP form into contact with the $\gamma$-phosphate and $Mg^{2+}$ ion. The changes in the corresponding region of EF-Tu are obscured by the absence, due to proteolysis, of 17 residues N-terminal to the conserved threonine in the EF-Tu$\cdot$GDP structure[11].

Likewise, the changes in the switch II region are also distinctly different. Although a portion of the switch II region is disordered

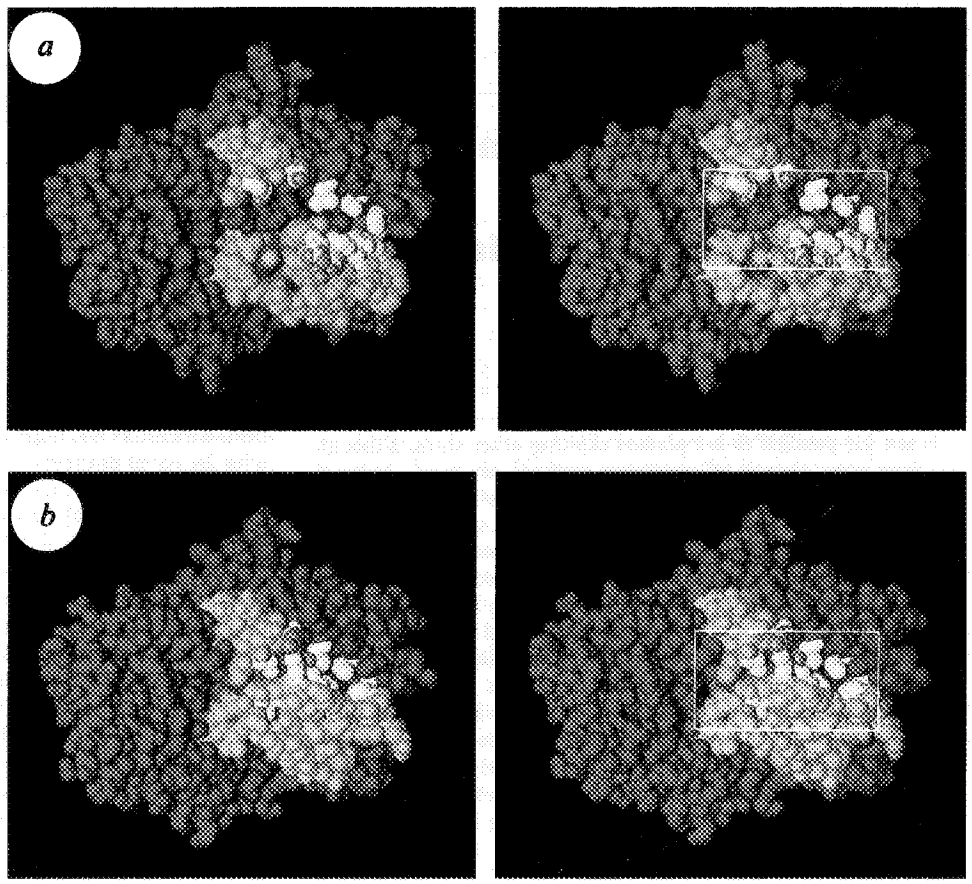


FIG. 4 Stereo pair of space filling models showing the same structures and view as in Fig. 1*b* and *c*. Residues in the switch regions are shown in cyan except for the gold residues which are those that propagate/stabilize the structural transitions induced by the $\gamma$-phosphate. The box outlines a cavity in $G_{t\alpha}\cdot$GDP that closes on introduction of GTP and may be a region of $G_{t\alpha}$ that along with the amino and carboxy termini modulates the affinity of $G_{t\alpha}$ for $G_{t\beta\gamma}$ and receptor. *a*, $G_{t\alpha}\cdot$GDP. *b*, $G_{t\alpha}\cdot$GTP-$\gamma$S.

in the GDP form of Ras, the conformational changes in the switch II region appear to resemble the changes in EF-Tu where GTP binding results in the addition of an extra helical turn at the carboxyl end of $\alpha 2$ at the expense of a turn at the beginning of the helix[12]. In conjunction with this, the $\alpha 2$ helix rotates by ~40° about an axis perpendicular to the helical axis. In $G_{t\alpha}$, rather than losing a turn at the beginning and gaining a turn at the end of $\alpha 2$, the GTP-induced changes straighten out an otherwise distorted $3_{10}$ helix while disrupting a reverse turn at the end of the helix. Furthermore, the rotation of the helical axis seen in p21 Ras and EF-Tu is replaced by a ~90° rotation roughly parallel to (but not coincident with) the helical axis. Finally, the partial unzipping of $\beta 3$–$\beta 1$ and concomitant extension of $\beta 3$–$\beta 2$ that couples the switch I and II regions in $G_{t\alpha}$, does not occur in either Ras[8–10] or EF-Tu[12]. Most distinctive is the presence in $G_{t\alpha}$ of a set of polar and nonpolar linkages that couple the primary structural changes, induced by interaction with the $\gamma$-phosphate, to nearby surface elements, some of which have been implicated in interactions with other components of the signalling system. Because these linkages are formed by residues that are unique to and conserved in $G_\alpha$ subunits we suggest that they provide the basis for a common switch mechanism in heterotrimeric G-protein-coupled signal transduction. □

Received 18 April; accepted 12 May 1994.


1. Hepler, J. R. & Gilman, A. G. *Trends Biochem. Sci.* **17,** 383–387 (1992).
2. Simon, M. I., Strathmann, M. P. & Gautam, N. *Science* **252,** 802–808 (1991).
3. Conklin, B. R. & Bourne, H. R. *Cell* **73,** 631–641 (1993).
4. Hurley, J. B. *J. Bioenerg. Biomembranes* **24,** 219–226 (1992).
5. Pfister, C. *et al. Cell Sig.* **5,** 235–241 (1993).
6. Hargrave, P. A. & Hamm, H. E. in *Molecular Pharmacoloy of Cell Regulation* Vol. 3 (eds Sibley, D. R. & Houslay, M. D.) 25–67 (Wiley, New York, 1994).
7. Bourne, H. R., Sanders, D. A. & McCormick, F. *Nature* **348,** 125–132 (1990).
8. Pai, E. F. *et al. Nature* **341,** 209–214 (1989).
9. Brunger, A. T. *et al. Proc. natn. Acad. Sci. U.S.A.* **87,** 4849–4853 (1990).
10. Tong, L. *et al. J. molec. Biol.* **217,** 503–516 (1991).
11. Jurnak, F. *Science* **230,** 32–36 (1985).
12. Berchtold, H. *et al. Nature* **365,** 126–132 (1993).
13. Noel, J. P., Hamm, H. E. & Sigler, P. B. *Nature* **366,** 654–663 (1993).
14. Mazzoni, M. R., Malinski, J. A. & Hamm, H. E. *J. biol. Chem.* **266,** 14072–14081 (1991).
15. Sternweis, P. C. & Gilman, A. C. *Proc. natn. Acad. Sci. U.S.A.* **79,** 4888–4891 (1982).
16. Fung, B. K.-K. & Nash, C. R. *J. biol. Chem.* **258,** 10503–10510 (1983).
17. Mazzoni, M. R. & Hamm, H. E. *J. Prot. Chem.* **12,** 215–221 (1993).
18. Higashijima, T. *et al. J. biol. Chem.* **262,** 752–756 (1987).
19. Faurobert, E. *et al. EMBO J.* **12,** 4191–4198 (1993).
20. Miller, R. T. *et al. Nature* **267,** 712–715 (1988).
21. Lee, E., Taussig, R. & Gilman, A. G. *J. biol. Chem.* **267,** 1212–1218 (1992).
22. Clark, K. L., Dignard, D., Thomas, D. Y. & Whiteway, M. *Molec. cell. Biol.* **13,** 1–8 (1993).
23. Whiteway, M. *et al. Molec. cell. Biol.* (in the press).
24. Thomas, T. C., Schmidt, C. J. & Neer, E. J. *Proc. natn. Acad. Sci. U.S.A.* **90,** 10295–10298 (1993).
25. Rarick, H. M., Artemyev, N. O. & Hamm, H. E. *Science* **256,** 1031–1033 (1992).
26. Berlot, C. H. & Bourne, H. R. *Cell* **68,** 911–922 (1992).
27. Stryer, L., Hurley, J. B. & Fung, B. K.-K. *Meth. Enzym.* **96,** 617–627 (1983).
28. Brunger, A. T. *Acta. crystallogr.* **A46,** 46–57 (1990).
29. Brunger, A. T. *X-PLOR Version 3.1 Manual* (Yale University, 1993).
30. Jones, T. A. *et al. Acta crystallogr.* **A47,** 110–119 (1991).
31. Jones, T. A. J. *J. appl. Crystallogr.* **11,** 268–276 (1978).
32. Yatsunami, K. & Khorana, H. G. *Proc. natn. Acad. Sci. U.S.A.* **82,** 4316–4320 (1985).
33. Robishaw, J. D. *et al. Proc. natn. Acad. Sci. U.S.A.* **83,** 1251–1255 (1986).
34. Nukada, T. *et al. FEBS Lett.* **197,** 305–308 (1986).
35. Van Meurs, K. P. *et al. Proc. natn. Acad. Sci. U.S.A.* **84,** 3107–3111 (1987).
36. Strathmann, M. & Simon, M. I. *Proc. natn. Acad. Sci. U.S.A.* **87,** 9113–9117 (1990).
37. Fong, H. K. W., Yoshimoto, K. K., Eversole-Cire, P. & Simon, M. I. *Proc. natn. Acad. Sci. U.S.A.* **85,** 3066–3070 (1988).
38. Nakafuku, M., Itoh, H., Nakamura, S. & Kaziro, Y. *Proc. natn. Acad. Sci. U.S.A.* **84,** 2140–2144 (1987).
39. Capon, D. J., Chen, E. Y., Levinson, A. D., Seeburg, P. H. & Goeddel, D. *Nature* **302,** 33–37 (1983).
40. Laursen, R. A., L'Italien, J. J., Nagarkatti, S. & Miller, D. L. *J. biol. Chem.* **256,** 8102–8109 (1981).
41. Fawzi, A. B. & Northrup, J. K. *Biochemistry* **29,** 3804–3812 (1990).
42. Higashijima, T. *et al. J. biol. Chem.* **262,** 762–766 (1987).
43. John, J., Frech, M. & Wittinghofer, A. *J. biol. Chem.* **263,** 11792–11799 (1988).
44. Kjeldgaard, M. & Nybord, J. *J. molec. Biol.* **223,** 721–742 (1992).


ACKNOWLEDGEMENTS. We thank R. Sweet and L. Berman of the Brookhaven National Lab for access to and help with the X-25 beam line at the NSLS, G. van Duyne, J. Geiger, J. Sondek and G. Ghosh for assistance during data collection, and C. Berlot, N. Artemyev and H. Dohlman for discussion. This work was supported by grants from the NIH to P.B.S. and H.E.H. H.E.H. was also supported by the American Heart Association and Research to Prevent Blindness. D.G.L. was a Damon Runyon postdoctoral fellow and J.P.N. was a NSF Chemistry and NIH postdoctoral fellow. The coordinates of $G_{t\alpha}$-GDP will be submitted to the Protein Data Bank.

LETTERS TO NATURE

# Dust depletion in the inner disk of β Pictoris as a possible indicator of planets

**P. O. Lagage & E. Pantin**

C.E.A., DSM, DAPNIA, Service d'Astrophysique, C.E. Saclay, F-91191 Gif-sur-Yvette Cédex, France

**IT is not yet possible to see planets orbiting other stars, although this may soon change as observing methods improve[1]. Indirect evidence for the presence of circumstellar dust disks out of which planets could form has been obtained for several stars, in the form of excess infrared emission, presumed to be from the hot dust[2,3]. Planets orbiting in such dust disks would be expected to sweep out dust-free tracks[4]. Indirect evidence for dust-free regions has been reported[5–9], based on an analysis of the spectral energy distribution, but the interpretation of the observation is not unique[7,9]. Here we present an infrared image of the inner dust disk of the star β Pictoris with a linear resolution of 5 astronomical units (AU), equivalent to the distance from the Sun to Jupiter. We find that the dust is asymmetrically distributed and is clearly depleted within 40 AU of the star, which we interpret as indicating the possible presence of at least one planetary body orbiting β Pictoris.**

The 10-μm region is one of the best spectral ranges to achieve high angular resolution for an object like the $\beta$ Pictoris disk. The outer part of the disk (>100 AU) has been first imaged with ground-based observations in the visible part of the spectrum[10]. But because of too high a contrast between the star and the disk emission, the disk structure within 2.5 arcsec of the star (40 AU at the distance of $\beta$ Pictoris, 16 pc) has been inaccessible until now, even with sophisticated techniques such as coronagraphic optics or anti-blooming CCDs (charge-coupled devices)[11,12]. Observing at 10 μm alleviates this problem, because the thermal emission from dust is comparable in intensity to the photospheric emission of the star, while the diffraction-limited angular resolution is still high: 0.7 arcsec for a 3-m telescope. This resolution, which has not been achieved with either single detectors or with arrays of discrete detectors[8,9] is now accessible with the new generation of integrated detector arrays. The European Southern Observatory (ESO) has recently acquired an instrument that employs such a device: the TIMMI camera, built by the Service d'Astrophysique at Saclay[13]. The detector is a monolithic 64 × 64 gallium-doped silicon array hybridized by indium bumps to a direct read out circuit, optimized by the LIR (Laboratoire Infra-Rouge) at the Grenoble Centre d'Etudes Nucléaires for the high-background conditions of ground-based broad-band imaging. The TIMMI camera mounted on the 3.6-m telescope at the ESO, La Silla, Chile was used during five nights (6–11 January 1993) for imaging the $\beta$ Pictoris dust disk at sub-arcsec resolution.

The disk structure observed after an on-source integration time of 75 min (spread over three nights) with a pixel field of view of 0.3 arcsec and a 10.5–13.3 μm band-pass filter is shown in Figs 1 (main figure) and 2; the signal-to-noise ratio at the